RESEARCH ARTICLE

CRYSTAL Research&Technology

www.crt-journal.org

Characterization of Elastic Constants of Langatate Single Crystals with 32 Symmetry Using Ultrasonic Pulse-Echo Technique

Chuanwen Chen, Lei Qin, Maoxin Su, Yang Xiang, Liguo Tang,* Kainan Xiong, Kechen Wu, Xiaoniu Tu,* and Wenyu Luo*

In this study, the propagation of plane waves in the lanthanum gallium tantalate (langatate, LGT) single crystals is investigated. Moreover, the flight time of different waves in the LGT rectangular parallelepiped sample is measured using the ultrasonic pulse-echo (UPE) technique, and the elastic constants of the LGT sample are determined. The experimental results clearly show echoes corresponding to the longitudinal and transverse waves along the *x*-axis. The waves along the *z*-axis have a similar property. However, the waves along the *y*-axis are more complex than those along the *x*- and *z*-axes. The echoes corresponding to the quasi-longitudinal waves along the *y*-axis are clear, but those corresponding to the transverse and quasi-transverse waves along the *y*-axis are not. The elastic constant can be accurately determined if the wave echoes corresponding to this constant propagate without distinct distortion and are clear; otherwise, it may be impossible to accurately determine the constant using UPE. All elastic constants c_{ij}^{E} except c_{13}^{E} of the LGT single crystals can be determined using UPE from one sample. This study uses UPE to provide a reference for the characterization of elastic constants of piezoelectric crystals with 32 symmetry from one sample.

1. Introduction

Lanthanum gallium tantalate (langatate, LGT) is considered a promising piezoelectric material for fabricating high-temperature transducers and sensors as well as langasite (LGS) and langanite (LGN).[1,2] They are also suitable for fabricating low-loss devices used in modern mobile communication and some other fields because 1) their piezoelectric properties are 2–3 times greater than those of α-quartz crystals; 2) the temperature has a weak influence on their elastic constants; and 3) they have an extremely high mechanical quality factor.[3,4] In addition, these crystals can be grown using the traditional Czochralski method,[2,5–7] enabling large-scale production.

LGT and its isomorphs belong to a trigonal system with 32 symmetry, whose independent material constants

C. Chen, Y. Xiang
Fujian Provincial Key Laboratory of Light Propagation and Transformation
College of Information Science and Engineering
Huaqiao University
Xiamen 361021, China
E-mail: cwchen@hqu.edu.cn

C. Chen, L. Tang, K. Wu
Fujian Key Laboratory of Functional Marine Sensing Materials
Minjiang University
Fuzhou 350108, China
E-mail: liguotang@xmu.edu.cn

L. Qin
Beijing Key Laboratory for Sensors
Beijing Information Science & Technology University
Beijing 100192, China

M. Su, K. Xiong, X. Tu
Shanghai Institute of Ceramics
Chinese Academy of Sciences
Shanghai 200050, China
E-mail: xiaoniu_tu@mail.sic.ac.cn

M. Su
Institute of Applied Micro-Nano Materials
School of Science
Beijing Jiaotong University
Beijing 100044, China

L. Tang, W. Luo
State Key Laboratory of Acoustics
Institute of Acoustics
Chinese Academy of Sciences
Beijing 100190, China

L. Tang
Key Laboratory of Underwater Acoustic Communication and Marine Information Technology
College of Ocean and Earth Sciences
Xiamen University
Xiamen 361010, China

The ORCID identification number(s) for the author(s) of this article can be found under https://doi.org/10.1002/crat.202400081

DOI: 10.1002/crat.202400081

include six elastic, two piezoelectric, and two dielectric constants. The LGT single crystals are suitable for fabricating high-temperature electromechanical devices because they can retain piezoelectricity up to their melting points of ≈1470 °C. Their material constants must be characterized before using them to design devices. Suhak et al.[8] studied the temperature-dependent acoustic loss in partially disordered LGS using a contactless tone-burst excitation technique and contacting resonant piezoelectric spectroscopy. Bohm et al.[9] obtained the elastic constants of LGS and LGT crystals using the ultrasonic pulse-echo (UPE) technique, then applied them to calculate and compare the phase velocities of the surface acoustic waves with the purpose of deriving optimized values for the elastic constants. Ju et al.[10] characterized the material constants of LGN crystals by UPE using multiple samples cut along different directions. Gureva et al.[11] measured the piezoelectric constant d_{11} of LGS crystals using the method of diffraction of synchrotron radiation. Note that the experiments based on the diffraction of synchrotron radiation are expensive. Most researchers are not available to carry out these experiments. Schreuer et al.[12] studied the elastic and piezoelectric properties of LGS and LGT crystals using resonant ultrasound spectroscopy (RUS). Theoretically, RUS needs only a single sample to characterize all elastic and piezoelectric constants. However, the material constant cannot be accurately determined by RUS if most resonance frequencies of the sample used in the characterization are not sensitive to its variation.

The UPE technique is one of the most powerful[13–16] methods for characterizing the elastic constants of solid materials. The elastic constants can be easily obtained using this technique by measuring the sound velocities.[17] However, only partial elastic constants can be determined using UPE from a single rectangular parallelepiped sample. Though all independent elastic constants of some piezoelectric crystals can be determined using UPE, multiple samples cut along different directions must be used in the characterization. This method is less commonly used because the preparation of these samples is difficult and time-consuming. Therefore, it is often used as an auxiliary tool for the electrical resonance and RUS methods, which are often used in the characterization of piezoelectric materials. The relationship between the electromechanical constants (including elastic, piezoelectric, and dielectric constants) and the bulk wave velocities should be derived before using UPE to investigate the elastic properties of piezoelectric samples. The Institution of Electrical and Electronic Engineers (IEEE) Standard on Piezoelectricity[18] presented the relationship between electromechanical constants and bulk wave velocities corresponding to piezoelectric materials with a ∞mm, 4 mm, or mm2 symmetry. Warner et al.[19] determined the material constants of $LiTaO_3$ and $LiNbO_3$ crystals with 3m symmetry using UPE. Chen et al.[17] obtained the elastic constants of the $[111]_c$ poled relaxor-based single crystals using the same technique. Though the elastic constants of LGT crystals have already been investigated using UPE,[9] some important problems have not yet been clarified, for example, the characteristics of the echoes corresponding to longitudinal and transverse waves propagating along different directions. Note that this determines which elastic constant can be accurately characterized using UPE.

In this study, the propagation of plane waves in LGT single crystals was investigated, and the relationship between their electromechanical constants and bulk wave velocities of LGT single crystals was derived. Moreover, echoes corresponding to longitudinal, quasi-longitudinal, transverse, and quasi-transverse waves along different axes of the LGT sample were measured and analyzed. Furthermore, all the elastic constants c_{ij}^{E} except c_{13}^{E} of the LGT sample were determined, and compared with those published. This study provides a reference for the characterization of all elastic constants c_{ij}^{E} except c_{13}^{E} of piezoelectric crystals with 32 symmetry from one sample using UPE.

2. Theory

The elastodynamic equations for piezoelectric crystals are formulated as follows:

$$\rho\frac{\partial^2 u_j}{\partial t^2} - c_{ijkl}^{E}\frac{\partial^2 u_k}{\partial x_i x_l} - e_{kij}\frac{\partial^2 \varphi}{\partial x_i x_k} = 0 \quad (i,j,k,l,=1,2,3) \tag{1}$$

and

$$e_{ikl}\frac{\partial^2 u_k}{\partial x_i x_l} - \varepsilon_{ik}^{S}\frac{\partial^2 \phi}{\partial x_i x_k} = 0 \quad (i,j,k,l,=1,2,3) \tag{2}$$

where ρ denotes the density, u_j denotes the displacement component, φ denotes the electric potential, c_{ijkl}^{E} denotes the elastic stiffness constant under a constant electric field, e_{ikl} denotes the piezoelectric stress constant, and ε_{ik}^{S} denotes the clamped dielectric constant.

The displacement components and electric potential corresponding to the plane harmonic waves in piezoelectric materials are

$$u_j = A_j\ \cos(\omega t - kl_n x_n), \quad (j,n\ =1,2,3) \tag{3}$$

$$\varphi\ = A_4\ \cos(\omega t - kl_n x_n), \quad (j,n\ =1,2,3) \tag{4}$$

where l_n denotes the cosine of the wave propagation direction and the axis x_n.

Substituting Equations (3) and (4) into Equations (1) and (2), we obtain

$$\rho v^2\ A_j = c_{ijkl}^{E}\ l_i l_l A_k + e_{kij} l_i l_k A_4 \tag{5}$$

$$-e_{ikl} l_i l_l A_k + \varepsilon_{ik} l_i l_k\ A_4 = 0 \tag{6}$$

Equations (5) and (6) are the well-known Christoffel equation[20] for piezoelectric crystals. They can be written as follows:

$$\begin{pmatrix} \Gamma_{11}-\rho v^2 & \Gamma_{12} & \Gamma_{13} & \Gamma_{14} \\ \Gamma_{21} & \Gamma_{22}-\rho v^2 & \Gamma_{23} & \Gamma_{24} \\ \Gamma_{31} & \Gamma_{23} & \Gamma_{33}-\rho v^2 & \Gamma_{34} \\ \Gamma_{41} & \Gamma_{24} & \Gamma_{43} & \Gamma_{44} \end{pmatrix}\begin{pmatrix} A_1 \\ A_2 \\ A_3 \\ A_4 \end{pmatrix} = 0 \tag{7}$$

where

$$\Gamma_{11} = c_{11}^{E}\ l_1 l_1 + c_{16}^{E} l_1 l_2 + c_{61}^{E} l_2 l_1 + c_{15}^{E} l_1 l_3 + c_{51}^{E} l_3 l_1 + c_{66}^{E} l_2 l_2 + c_{65}^{E} l_2 l_3 + c_{56}^{E} l_3 l_2 + c_{55}^{E} l_3 l_3 \tag{8}$$

$$\Gamma_{22} = c^{E}_{66}\, l_1 l_1 + c^{E}_{62} l_1 l_2 + c^{E}_{26} l_2 l_1 + c^{E}_{64} l_1 l_3 + c^{E}_{46} l_3 l_1 + c^{E}_{22} l_2 l_2 + c^{E}_{24} l_2 l_3 + c^{E}_{42} l_3 l_2 + c^{E}_{44} l_3 l_3 \quad (9)$$

$$\Gamma_{33} = c^{E}_{55}\, l_1 l_1 + c^{E}_{54} l_1 l_2 + c^{E}_{45} l_2 l_1 + c^{E}_{53} l_1 l_3 + c^{E}_{35} l_3 l_1 + c^{E}_{44} l_2 l_2 + c^{E}_{43} l_2 l_3 + c^{E}_{34} l_3 l_2 + c^{E}_{33} l_3 l_3 \quad (10)$$

$$\Gamma_{44} = -\left[\varepsilon_{11} l_1 l_1 + \varepsilon_{12} l_1 l_2 + \varepsilon_{21} l_2 l_1 + \varepsilon_{13} l_1 l_3 + \varepsilon_{31} l_3 l_1 + \varepsilon_{22} l_2 l_2 + \varepsilon_{23} l_2 l_3 + \varepsilon_{32} l_3 l_2 + \varepsilon_{33} l_3 l_3\right] \quad (11)$$

$$\Gamma_{12} = \Gamma_{21} = c^{E}_{16}\, l_1 l_1 + c^{E}_{12} l_1 l_2 + c^{E}_{66} l_2 l_1 + c^{E}_{14} l_1 l_3 + c^{E}_{56} l_3 l_1 + c^{E}_{62} l_2 l_2 + c^{E}_{64} l_2 l_3 + c^{E}_{52} l_3 l_2 + c^{E}_{54} l_3 l_3 \quad (12)$$

$$\Gamma_{13} = \Gamma_{31} = c^{E}_{15}\, l_1 l_1 + c^{E}_{14} l_1 l_2 + c^{E}_{65} l_2 l_1 + c^{E}_{13} l_1 l_3 + c^{E}_{55} l_3 l_1 + c^{E}_{64} l_2 l_2 + c^{E}_{63} l_2 l_3 + c^{E}_{54} l_3 l_2 + c^{E}_{53} l_3 l_3 \quad (13)$$

$$\Gamma_{14} = \Gamma_{41} = e_{11}\, l_1 l_1 + e_{21} l_1 l_2 + e_{16} l_2 l_1 + e_{31} l_1 l_3 + e_{15} l_3 l_1 + e_{26} l_2 l_2 + e_{36} l_2 l_3 + e_{25} l_3 l_2 + e_{35} l_3 l_3 \quad (14)$$

$$\Gamma_{23} = \Gamma_{32} = c^{E}_{65}\, l_1 l_1 + c^{E}_{64} l_1 l_2 + c^{E}_{25} l_2 l_1 + c^{E}_{63} l_1 l_3 + c^{E}_{45} l_3 l_1 + c^{E}_{24} l_2 l_2 + c^{E}_{23} l_2 l_3 + c^{E}_{44} l_3 l_2 + c^{E}_{43} l_3 l_3 \quad (15)$$

$$\Gamma_{24} = \Gamma_{42} = e_{16}\, l_1 l_1 + e_{26} l_1 l_2 + e_{12} l_2 l_1 + e_{36} l_1 l_3 + e_{14} l_3 l_1 + e_{22} l_2 l_2 + e_{32} l_2 l_3 + e_{24} l_3 l_2 + e_{34} l_3 l_3 \quad (16)$$

$$\Gamma_{34} = \Gamma_{43} = e_{15}\, l_1 l_1 + e_{25} l_1 l_2 + e_{14} l_2 l_1 + e_{35} l_1 l_3 + e_{13} l_3 l_1 + e_{24} l_2 l_2 + e_{34} l_2 l_3 + e_{23} l_3 l_2 + e_{33} l_3 l_3 \quad (17)$$

The necessary and sufficient condition for Equation (7) to have nontrivial solutions is that the determinant of its coefficient matrix must equal zero. Three different waves were traveling in each direction. In general, the displacement vectors of the three waves were neither perpendicular nor parallel to their propagation direction. However, pure-mode waves appeared when the crystal was highly symmetrical with respect to the propagation direction.

By substituting Equation (6) into Equation (5), we can reduce the four equations to the following:

$$\left[c^{D'}_{ijkl} l_i l_l A_k - \rho v^2 \delta_{jk}\right] A_k = 0, \quad (i,j,k,l = 1,2,3) \quad (18)$$

where

$$\delta_{jk} = \begin{cases} 0 & j \neq k \\ 1 & j = k \end{cases} \quad (19)$$

$$c^{D'}_{ijkl} = c^{E}_{ijkl} + e_{lij} \frac{e_{mkn} l_m l_n}{\varepsilon_{pq} l_p l_q}, \quad (i,j,k,l,m,n,p,q = 1,2,3) \quad (20)$$

Equation (18) has the same form as that of a nonpiezoelectric material. The constant $c^{D'}_{ijkl}$ is not the same as the elastic stiffness constant under a constant electric displacement c^{D}_{ijkl}. Usually, the elastic constant c_{ijkl} ($i, j, k, l = 1, 2, 3$) is abbreviated as c_{ij} ($i, j = 1, 2, \ldots, 6$) using compressed subscripts. For example, c_{1221}, c_{1212}, c_{2121}, and c_{2112} are abbreviated as c_{66}. However, this method is not suitable for $c^{D'}_{ijkl}$. The constants $c^{D'}_{1221}$, $c^{D'}_{1212}$, $c^{D'}_{2121}$, and $c^{D'}_{2112}$ in Equation (20) has different meanings, as discussed in Section 4.1.

The LGT crystal structure belongs to a trigonal system with 32 symmetry. Its full matrix constants are formulated as follows:

$$[c^{E}] = \begin{bmatrix} c^{E}_{11} & c^{E}_{12} & c^{E}_{13} & c^{E}_{14} & 0 & 0 \\ c^{E}_{12} & c^{E}_{11} & c^{E}_{13} & -c^{E}_{14} & 0 & 0 \\ c^{E}_{13} & c^{E}_{13} & c^{E}_{33} & 0 & 0 & 0 \\ c^{E}_{14} & -c^{E}_{14} & 0 & c^{E}_{44} & 0 & 0 \\ 0 & 0 & 0 & 0 & c^{E}_{44} & c^{E}_{14} \\ 0 & 0 & 0 & 0 & c^{E}_{14} & c^{E}_{66} \end{bmatrix} \quad (21)$$

$$[e] = \begin{bmatrix} e_{11} & -e_{11} & 0 & e_{14} & 0 & 0 \\ 0 & 0 & 0 & 0 & -e_{14} & -e_{11} \\ 0 & 0 & 0 & 0 & 0 & 0 \end{bmatrix} \quad (22)$$

$$[\varepsilon^{S}] = \begin{bmatrix} \varepsilon^{S}_{11} & 0 & 0 \\ 0 & \varepsilon^{S}_{11} & 0 \\ 0 & 0 & \varepsilon^{S}_{33} \end{bmatrix} \quad (23)$$

where $c^{E}_{66} = \frac{1}{2}(c^{E}_{11} - c^{E}_{12})$.

Equation (18) can be simplified significantly when the wave propagates along the x-, y-, or z-axis. For the waves traveling along the z-axis ($l_1 = 0,\ l_2 = 0, l_3 = 1$), we have

$$\begin{pmatrix} c^{E}_{44} - \rho v^2 & 0 & 0 \\ 0 & c^{E}_{44} - \rho v^2 & 0 \\ 0 & 0 & c^{E}_{33} - \rho v^2 \end{pmatrix} \begin{pmatrix} A_1 \\ A_2 \\ A_3 \end{pmatrix} = 0 \quad (24)$$

There is a one-to-one correspondence between the two elastic constants and two wave velocities in Equation (24), i.e.,

$$c^{E}_{33} = \rho (v^{z}_{L})^2, \quad c^{E}_{44} = \rho (v^{z}_{Tx})^2 = \rho (v^{z}_{Ty})^2 \quad (25)$$

where the superscript z represents the wave propagation direction, the subscripts x and y represent the directions of particle vibration, and the subscripts L and T represent longitudinal and transverse waves, respectively.

3. Experimental Section

The LGT single crystal was grown along the X-axis using an Ir crucibles by the Czochralski method. The growth atmosphere was nitrogen with 1–2 Vol% oxygen. The pulling rate was 0.6–3 mm h^{-1}, and the rotation rate was varied from 10 to 30 rpm. The as-grown crystal was pale orange in color. Its diameter and thickness are 82 and 100 mm, respectively. The LGT sample was orientated using the Laue method with an accuracy of ± 0.5°, and cut in the principal x-y-z directions. The dimensions of the sample

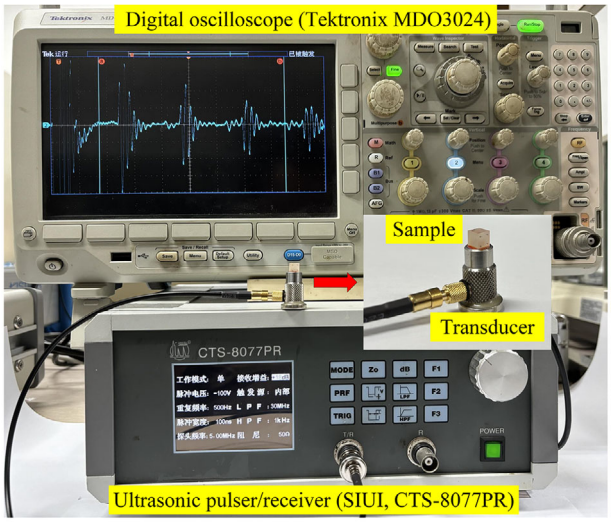

Figure 1. Ultrasonic pulse-echo setup.

were 5.000 × 5.040 × 5.078 mm^3, which were measured using a digital micrometer (Mikrometry DHG-050). Its density was measured using the Archimedes method to be equal to 6129 kg m^{-3}. All bulk waves along the *x*-, *y*-, and *z*-axes were measured using the UPE setup shown in **Figure 1**. An ultrasonic transducer was connected to an ultrasonic pulser/receiver (SIUI, CTS-8077PR). The sample was put onto the transducer surface. The ultrasonic echoes propagating in the sample were shown in a digital oscilloscope (Tektronix MDO3024) with a bandwidth of 200 MHz, which was connected to the pulser/receiver. A 5 MHz shear transducer (Olympus V156RM) and a 10 MHz longitudinal (Olympus CN10R-5) transducer were used to excite and receive longitudinal and transverse waves, respectively. The -3 dB bandwidth of the Olympus CN10R-5 transducer ≈60%. The −6 dB bandwidth of the Olympus V156RM transducer ≈66%.

4. Results and Discussion

4.1. Waves Traveling in the x-y Plane

The waves traveling along the *x*- or *y*-axis, whose vibration direction is neither perpendicular nor parallel to the axis, are more complex than those traveling along the *z*-axis. To understand the waves traveling along the *x*- or *y*-axis better, bulk waves traveling in the *x*-*y* plane were investigated. In this case, l_1, l_2, and l_3 in Equations (8)–(17) equal cosθ, sinθ, and 0, respectively, where θ is the angle between the wave propagation direction and the *x*-axis. The matrix elements in Equation (7) can be simplified when $l_3 = 0$. The constants $c_{ijkl}^{D'}$ in Equations (18)–(20) also can be simplified significantly. For example, $c_{1221}^{D'}$, $c_{1212}^{D'}$, $c_{2121}^{D'}$, and $c_{2112}^{D'}$ can be written as

$$c_{1221}^{D'} = c_{2121}^{D'} = c_{66}^{E} \tag{26}$$

$$c_{2112}^{D'} = c_{1212}^{D'} = c_{66}^{E} + \frac{p}{r}e_{26} \tag{27}$$

where

$$p = e_{11}\,l_1l_1 + e_{26}l_2l_2,\ r = \varepsilon_{11}\,l_1l_1 + \varepsilon_{22}l_2l_2 \tag{28}$$

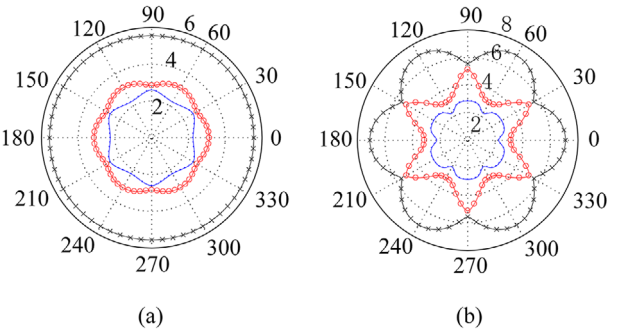

Figure 2. Velocity curves of crystals in the *x*-*y* plane. a) Original LGT crystal; b) LGT crystal with piezoelectric constants multiplied by 10. The unit of velocity is km s^{-1} (the black line corresponds to a longitudinal (or quasi-longitudinal) wave, and the red and blue lines correspond to two transverse (or quasi-transverse) waves).

Equations (26) and (27) indicate that $c_{1221}^{D'}$ and $c_{2112}^{D'}$ have different meanings. Consequently, $c_{1221}^{D'}$, $c_{1212}^{D'}$, $c_{2121}^{D'}$, and $c_{2112}^{D'}$ cannot be represented by the same compressed subscript symbol $c_{66}^{D'}$. Therefore, the compressed subscripts cannot be used in $c_{ijkl}^{D'}$ in some complicated cases.

The variation in the velocity of waves traveling in the *x*-*y* plane with the propagation direction for the LGT crystals is shown in **Figure 2**a. A longitudinal or quasi-longitudinal wave has the largest propagation velocity, which hardly changes with the propagation direction, as shown in Figure 2a. To study the effect of the piezoelectric properties of piezoelectric single crystals with 32 symmetry on the wave velocity, we artificially increased the piezoelectric coefficients of the LGT crystals to 10 times those of the original crystals. The results are presented in Figure 2b. The velocity curves of the longitudinal and quasi-longitudinal waves also exhibited hexangular symmetry. Comparing Figure 2b with Figure 2a, we observe that the higher the piezoelectric coefficients, the stronger the influence of the propagation direction on the wave velocity.

4.2. Waves Traveling Along the x-Axis

For waves traveling along the *x*-axis in the LGT crystals, we have $l_1 = 1$, $l_2 = 0$, and $l_3 = 0$, where one longitudinal wave L^x and two transverse waves T_1^x and T_2^x exist. The displacement vectors corresponding to these two transverse waves were not parallel to the *y* or *z*-axis, as shown in **Figure 3**

Moreover, their velocities were determined by several elastic constants rather than a single elastic constant. The elastic constants associated with the two wave velocities v_{T1}^x and v_{T2}^x are labeled c_1^E and c_2^E, respectively. From Equation (7), we have

$$c_{11}^{D} = \rho(v_L^x)^2, \quad c_1^E = \rho(v_{T1}^x)^2, \quad c_2^E = \rho(v_{T2}^x)^2 \tag{29}$$

where

$$c_{11}^{D} = c_{11}^{E} + \frac{e_{11}^2}{\varepsilon_{11}} \tag{30}$$

$$c_1^E = \frac{1}{2}\left[\left(c_{44}^E + c_{66}^E\right) + \sqrt{\left(c_{44}^E - c_{66}^E\right)^2 + 4\left(c_{14}^E\right)^2}\right] \tag{31}$$

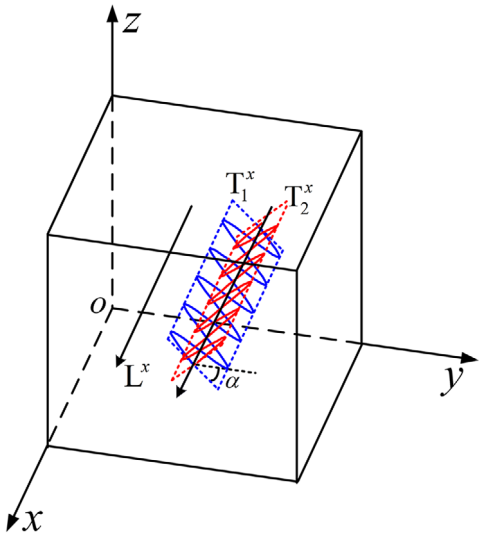

Figure 3. Schematic diagram of T_1^x and T_2^x when waves are propagating along the x direction.

$$c_2^E = \frac{1}{2}\left[\left(c_{44}^E + c_{66}^E\right) - \sqrt{\left(c_{44}^E - c_{66}^E\right)^2 + 4\left(c_{14}^E\right)^2}\right] \tag{32}$$

where c_{ij}^D is the elastic stiffness constant under the constant electric displacement.

Considering the two transverse waves T_1^x and T_2^x, we substituted c_1^E and c_2^E into Equation (7), and the vibration amplitudes can be written as follows:

$$\frac{A_2}{A_3} = \frac{c_{14}^E}{c_1^E - c_{66}^E} \quad (\text{for } T_1^x) \tag{33}$$

$$\frac{A_2}{A_3} = \frac{c_{14}^E}{c_2^E - c_{66}^E} \quad (\text{for } T_2^x) \tag{34}$$

The vibration direction of these two waves can be written in vector forms as

$$\mathbf{r}_1 = c_{14}^E\,\mathbf{j} + \left(c_1^E - c_{66}^E\right)\mathbf{k} \quad (\text{for } T_1^x) \tag{35}$$

$$\mathbf{r}_2 = c_{14}^E\,\mathbf{j} + \left(c_2^E - c_{66}^E\right)\mathbf{k} \quad (\text{for } T_2^x) \tag{36}$$

It is easy to prove that the dot product of these two vectors equals zero, i.e., $\mathbf{r}_1 \cdot \mathbf{r}_2 = 0$. Therefore, the vibration directions of the two transverse waves were perpendicular to each other. The angle α between the displacement of T_1^x and the y-axis can be calculated using

$$\tan\alpha = \left|\frac{c_1^E - c_{66}^E}{c_{14}^E}\right| \tag{37}$$

Conversely, α can be measured using UPE. If the value of α can be measured accurately, then the accuracy of the determined elastic stiffness constants can be evaluated by comparing the calculated and measured values of α. By repeating the aforementioned analysis, we can prove that the vibration directions of the quasi-longitudinal and quasi-transverse waves are also perpendicular to each other when the propagation direction is along the y-axis.

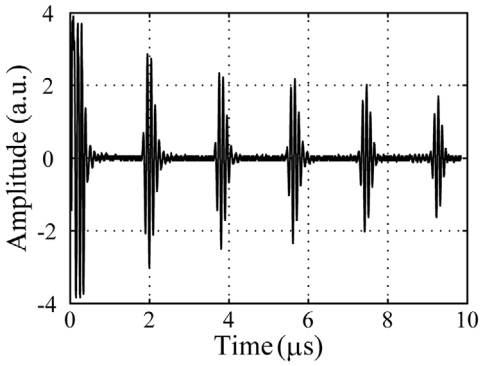

Figure 4. Sample pulses of a longitudinal wave in LGT crystal traveling along the x-axis.

Table 1. Phase velocities of different waves were measured using UPE and corresponding elastic constants for LGT crystals with 32 symmetry.

Waves	L^x	T_1^x	T_2^x	QL^y	T_x^y	QT_z^y	L^z	T_x^z, T_y^z
v (m s^{-1})	5594	3124	2126	5572	–	2931	6544	2891
Elastic constants c	c_{11}^D	c_1^E	c_2^E	c_3^E	c_{66}^D	c_4^E	c_{33}^E	c_{44}^E
Values of c (10^{10} N/m^2)	19.18	6.031	2.988	19.03	–	5.266	26.25	5.122

The piezoelectric constants c_n^D $(n = 1, 2, 3, 4)$ for piezoelectric single crystals with $3m$ symmetry have the same form as c_n^E for piezoelectric single crystals with 32 symmetry. Replacing all the superscripts "E" in Equations (31) and (32) with "D," we obtained the expression of c_n^D corresponding to single crystals with $3m$ symmetry. The echoes of the longitudinal wave L^x shown in **Figure 4** are very clear. Moreover, the first five echoes shown in Figure 4 are barely distorted. Therefore, the round-trip flight time was precisely measured. Consequently, the phase velocity of the wave L^x and corresponding elastic stiffness constant c_{11}^D were accurately determined, as shown in **Table 1**.

As mentioned previously, for the two transverse waves traveling along the x-axis, their vibrations were not parallel to the y- or z-axis. **Figure 5**a,b shows that multiple echoes occurred when the shear transducer vibrating along y- or z-axis was used to excite a pulse traveling along the x-axis of the LGT sample. Both the T_1^x and T_2^x echoes are shown in Figure 5a,b. However, it is difficult to identify the T_2^x echoes from them. When measuring the transverse waves traveling along the x-axis, clear echoes of the transverse waves can be found in two directions by rotating the shear transducer in the y-z plane. These two directions correspond to the particle vibration directions of transverse waves T_1^x and T_2^x. The round-trip flight times corresponding to the T_1^x wave can be accurately measured because its echoes propagate without distinct distortion and are clear, as shown in Figure 5c). The velocity of the T_1^x wave, i.e., v_{T1}^x, can then be accurately determined, as listed in Table 1. Furthermore, the elastic constant c_1^E can be accurately determined using Equation (29), as listed in Table 1. However, the waveform of the first echo of the T_2^x wave is different from that of its second echo, which shows that it propagated

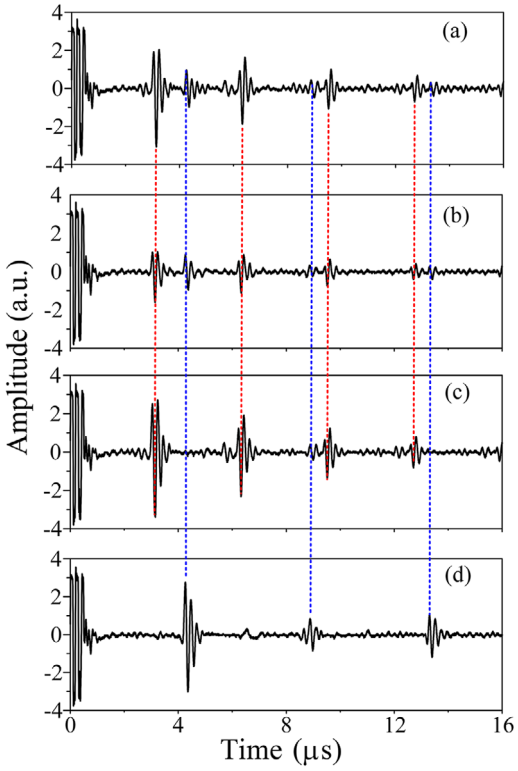

Figure 5. Two transverse waves traveling along the *x*-axis with the transducer vibrating along a) *y*-axis, b) *z*-axis, c) vibration direction of T_1^x, and d) the vibration direction of T_2^x. The red dashed lines denote the echoes of T_1^x wave at the same phase. The blue dashed lines denote the echoes of T_2^x wave at the same phase.

with distortion. Therefore, it is difficult to accurately measure the round-trip flight time. To reduce the measurement error, the time interval between the first and third echoes was measured to calculate the wave velocity, as denoted with blue dashed line in Figure 5d. Nevertheless, the measurement error of c_2^E may be slightly large.

4.3. Waves Traveling Along the y-Axis

Three kinds of waves are traveling along the *y*-axis in the LGT crystals, namely, pure transverse waves denoted as T_x^y, quasi-transverse waves denoted as QT_Z^y, and quasi-longitudinal waves denoted as QL^y. The relationships between the velocities and the elastic constants are as follows:

$$c_{66}^D = \rho(v_{Tx}^y)^2,\ c_3^E = \rho(v_{QL}^y)^2,\ c_4^E = \rho(v_{QT}^y)^2 \tag{38}$$

where

$$c_{66}^D = c_{66}^E + \frac{e_{26}^2}{\varepsilon_{22}} \tag{39}$$

$$c_3^E = \frac{1}{2}\left[\left(c_{11}^E + c_{44}^E\right) + \sqrt{\left(c_{11}^E - c_{44}^E\right)^2 + 4\left(c_{14}^E\right)^2}\right] \tag{40}$$

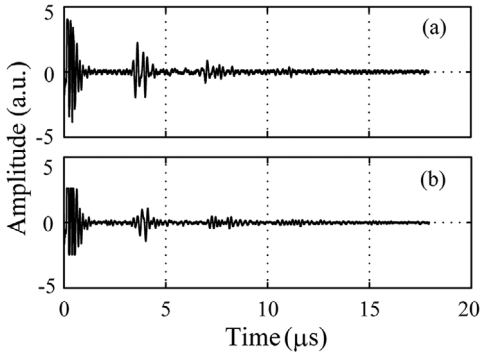

Figure 6. Waves travel along the *y*-axis when the shear transducer vibrates along a) *z*-axis and b) *x*-axis.

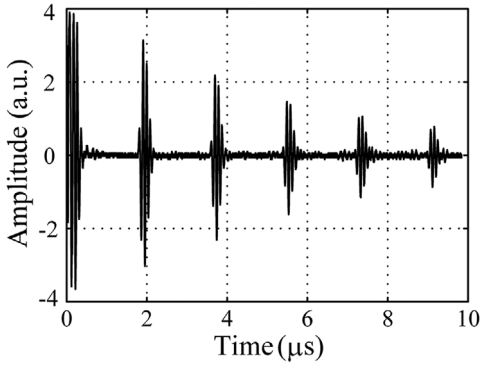

Figure 7. Quasi-longitudinal wave in LGT crystal traveling along the *y*-axis.

$$c_4^E = \frac{1}{2}\left[\left(c_{11}^E + c_{44}^E\right) - \sqrt{\left(c_{11}^E - c_{44}^E\right)^2 + 4\left(c_{14}^E\right)^2}\right] \tag{41}$$

where v_{Tx}^y, v_{QL}^y, and v_{QT}^y are velocities of pure transverse, quasi-longitudinal, and quasi-transverse waves, respectively.

The T_x^y and QT_Z^y echoes were detected using a shear transducer. When the transducer vibrated transversely along the *z*- or *x*-axis, no clear series of echoes was observed, as shown in **Figure 6**. We note that quasi-longitudinal waves QL^y also exist in the *y*-*z* plane. Both QT_Z^y and QL^y waves have vibration components in the *z*-axis direction. Therefore, when the transducer vibrated transversely along the *z*-axis, the echoes of these two waves were detected simultaneously. This may have caused the echoes to become more complex. By contrast, both quasi-transverse and quasi-longitudinal waves may occur in the reflected waves after the quasi-transverse or quasi-longitudinal waves are reflected by the boundary surface of the sample.[21,22] Consequently, the echoes shown in Fig. 6 became more complex, which makes the measurement of the time of flight between two echoes shown in Figure 6 subject to large errors. Therefore, the values of c_4^E and c_{66}^D characterized using Equation (38) are likely to have large errors, as shown in Table 1. The value of c_4^E calculated using Equation (41) is 4.982×10^{10} N m^{-2}. The relative deviation between this value and that in Table 1 reaches 5%.

No pure longitudinal wave traveled along the *y*-axis. A quasi-longitudinal wave QL^y exists. The first three echoes are clear and without distinct distortion, as shown in **Figure 7**. Therefore, the corresponding elastic constant c_3^E can be accurately determined

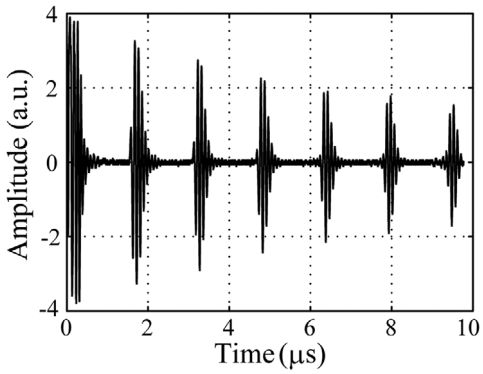

Figure 8. Longitudinal wave in LGT crystal traveling along *z*-axis.

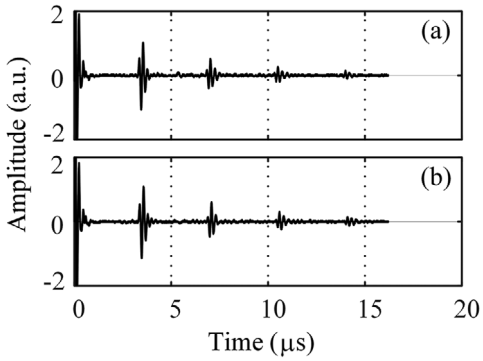

Figure 9. Transverse waves a) T_x^z and b) T_y^z traveling along *z*-axis.

using these echoes. The value of c_3^E is determined from c_{11}^E, c_{14}^E, and c_{44}^E, as shown in Equation (40). Theoretically, the longitudinal mode transducer can also be used to detect the echoes of quasi-transverse waves.

4.4. Waves Traveling Along the z-Axis

According to Equation (25), a pure longitudinal plane wave traveling along the z-axis can be excited using a longitudinal transducer, which is denoted as L^z. Moreover, two pure transverse plane waves traveling along the z-axis can be excited using a shear transducer, which is denoted as T_x^z and T_y^z. The subscripts x and y represent the vibration direction. The longitudinal wave echoes are shown in **Figure 8**. Based on these echoes, the elastic constant c_{33}^E can be accurately determined because first four echoes are very clear and without distinct distortion. The echoes of the two transverse waves are shown in **Figure 9**, from which the time interval between two adjacent echoes can be obtained. Then the phase velocity corresponding to these waves can be determined. Furthermore, we can calculate the value of the elastic constant c_{44}^E based on Equation (25).

Other elastic constants can be derived from the obtained results. From Equations (29) and (30), we obtain

$$c_{66}^E = c_1^E + c_2^E - c_{44}^E \tag{42}$$

and

$$c_{14}^E = \sqrt{c_{44}^E c_{66}^E - c_1^E c_2^E} \tag{43}$$

Table 2. Elastic constants (10^{10} N m^{-2}) of LGT single crystals.

Elastic constants (10^{10} N m^{-2})	This study	References [9]	References [12]
c_{11}^E	18.88	18.89	18.88
c_{12}^E	11.08	10.86	10.78
c_{13}^E	–	10.44	10.02
c_{14}^E	1.394	1.374	1.350
c_{33}^E	26.25	26.45	26.11
c_{44}^E	5.122	5.129	5.095
c_{66}^E	3.897	4.019	4.050

c_{66}^E and c_{14}^E can be determined by substituting the values of c_1^E, c_2^E, and c_{44}^E into Equations (42) and (43).

Moreover, c_{11}^E can be determined precisely by substituting the values of c_3^E, c_{14}^E, and c_{44}^E into Equation (40). Additionally, c_{12}^E can be determined using $c_{12}^E = c_{11}^E - 2c_{66}^E$. In other words, all the elastic constants c_{ij}^E except c_{13}^E of the LGT single crystals can be determined.

For comparison, the elastic constants of LGT single crystals obtained in this study and those presented in Refs. [9, 12] were listed in **Table 2**. In Ref. [9], the elastic constants obtained using UPE were used to calculate and compare the phase velocities of the surface acoustic waves with the purpose of deriving optimized values for the elastic constants of LGT crystals. In Ref. [9], the RUS method was used to characterize the elastic and piezoelectric constants of LGT crystals. The value of c_{13}^E is determined by c_{11}^E, c_{14}^E, c_{33}^E, c_{44}^E and the phase velocity of a wave propagating in a rotated Y-cut LGT sample in Ref. [9]. Therefore, their measurement errors probably transfer to c_{13}^E, which may lead to a large characterization error. Table 2 shows that the relative deviation between the values of c_{13}^E presented in Refs. [9, 12] reaches 4%. The values of c_{11}^E obtained in this study and Refs. [9, 12] agree well, as well as c_{33}^E and c_{44}^E. However, the relative deviation between the values of c_{66}^E obtained in this study and Ref. [9] reaches 3%, and that between the values of c_{66}^E obtained in this study and Ref. [12] reaches 4%. The error of c_{66}^E probably be mainly from that of c_2^E, as illustrated in Section 4.2.

5. Conclusion

Bulk waves traveling in LGT single crystals with 32 symmetry were investigated systematically. Ferroelectric single crystals with 32 symmetry have the same elastic and dielectric constant matrices as those with 3*m* symmetry; however, they have different piezoelectric constant matrices. For example, the piezoelectric constants d_{31}, d_{32}, and d_{33} of ferroelectric single crystals with 32 symmetry are equal to zero; however, these constants are nonzero for ferroelectric single crystals with 3*m* symmetry. Therefore, ferroelectric single crystals with 32 and 3*m* symmetries have different relationships between the bulk wave velocities and the electromechanical constants.

The relationships between the velocities corresponding to the different waves traveling along the *x*-, *y*-, and *z*-axes, and the electromechanical constants corresponding to the LGT crystals were derived. Furthermore, characterizing the elastic constants of LGT crystals using UPE was investigated. The echoes of the longitudinal (or quasi-longitudinal) waves traveling along the *x*-,

y- and z-axes, as well as the transverse waves traveling along the x- and z-axes, were extremely clear. Therefore, the elastic constants c_{11}^{D}, c_{1}^{E}, c_{3}^{E}, c_{33}^{E}, and c_{44}^{E} could be directly determined with high accuracy. Note that the echoes correspond to c_{2}^{E} was clear, however, the echoes propagated with distortion, which led a slightly large error of the characterized c_{2}^{E}. The echoes of the two transverse (or quasi-transverse) waves traveling along the y-axis could not be measured clearly. Consequently, the round-trip flight times corresponding to these waves could not be determined precisely. Therefore, the c_{4}^{E} and c_{66}^{D} levels could not be precisely determined. Though c_{13}^{E} can be determined using one more rotated Y-cut sample by UPE, the characterization error may be large. The reason is that the value of c_{13}^{E} is not only determined by the phase velocity of the wave propagating in the rotated Y-cut sample but also by c_{11}^{E}, c_{14}^{E}, c_{33}^{E} and c_{44}^{E}. Their errors will transfer to the determined value of c_{13}^{E}. To obtain its more accurate value, RUS is a good alternative. Moreover, RUS can determine the temperature dependence of all elastic constants of LGT crystals. Note that c_{66}^{E} and c_{14}^{E} can be determined by substituting the values of c_{1}^{E}, c_{2}^{E}, and c_{44}^{E} into Equations (33) and (34). The error of c_{2}^{E} may be slightly large, which is the main contribution of the characterization error of c_{66}^{E}. Moreover, c_{11}^{E} can be determined precisely by substituting the values of c_{3}^{E}, c_{14}^{E}, and c_{44}^{E} into Equation (31). Additionally, c_{12}^{E} can be determined using $c_{12}^{E} = c_{11}^{E} - 2c_{66}^{E}$. In other words, all the elastic constants c_{ij}^{E} except c_{13}^{E} of the LGT single crystals can be determined using UPE from one sample.

Acknowledgements

This work was supported by the National Natural Science Foundation of China (Grant Nos. 12274358 and U2006218), State Key Laboratory of Acoustics, Chinese Academy of Science (Grant No. SKLA202309), the Project of Construction and Support for High-level Innovative Teams of Beijing Municipal Institutions (BPHR20220124), Qin Xin Talents Cultivation Program, Beijing Information Science & Technology University (QXTCP A202103), and Fujian Key Laboratory of Functional Marine Sensing Materials, Minjiang University (MJUKF-FMSM202207).

Conflict of Interest

The authors declare no conflict of interest.

Author Contributions

C.C. performed formal analysis, and wrote the original draft. L.Q. performed conceptualization, and aquired funding acquisition, M.S. performed methodology, and sample preparation. Y.X. performed data curation, and validation. L.T. performed conceptualization, and acquired funding acquisition, and wrote - review and perform editing. K.X. performed investigation. K.W. performed data curation. X.T. performed methodology, data curation, and sample preparation. W.L. wrote - review and perform editing.

Data Availability Statement

The data that support the findings of this study are available from the corresponding author upon reasonable request.

Keywords

elastic constants, langatate single crystals, piezoelectric constants, ultrasonic pulse-echo

Received: March 20, 2024
Revised: July 18, 2024
Published online:

[1] H. Fritze, *J. Electroceram.* **2011**, *26*, 122.
[2] S. Wang, C. Ji, P. Dai, G. Guo, L. Shen, N. Bao, *Mater. Res. Bull.* **2022**, *152*, 111848.
[3] M. Allani, N. Batis, T. Laroche, A. Nehari, H. Cabane, K. Lebbou, X. Vacheret, J. J. Boy, *Adv. Appl. Ceram.* **2018**, *117*, 279.
[4] M. P. da Cunha, D. C. Malocha, E. L. Adler, K. J. Casey, *IEEE T Ultrason. Ferr.* **2002**, *49*, 1291.
[5] J. Bohm, R. B. Heimann, M. Hengst, R. Roewer, J. Schindler, *J. Cryst. Growth* **1999**, *204*, 128.
[6] H. Takeda, Y. Sobata, H. Usui, S. Kodama, I. Yanase, T. Hoshina, T. Tsurumi, K. Shimamura, *J. Ceram. Soc. Jpn.* **2022**, *130*, 16.
[7] A. Nehari, G. Alombert-Goget, O. Benamara, H. Cabane, M. Dumortier, P. Jeandel, I. Lasloudji, F. Mokhtari, T. Baron, G. Wong, M. Allani, J. Boy, S. Alzuaga, L. Arapan, F. Gegot, T. Dufar, K. Lebbou, *Cryst. Eng. Comm.* **2019**, *21*, 1764.
[8] Y. Suhak, H. Fritze, A. Sotnikov, H. Schmidt, W. L. Johnson, *J. Appl. Phys.* **2021**, *130*, 085102.
[9] J. Bohm, E. Chilla, C. Flannery, H. J. Frohlich, T. Hauke, R. B. Heimann, M. Hengst, U. Straube, *J. Cryst. Growth* **2000**, *216*, 293.
[10] S. Ju, H. Zhang, J. A. Kosinski, *IEEE T Ultrason. Ferr.* **2022**, *69*, 2137.
[11] P. V. Gureva, N. V. Marchenkov, A. N. Artemev, N. A. Artemiev, A. D. Belyaev, A. A. Demkiv, V. A. Shishkov, *J. Appl. Crystallogr.* **2020**, *53*, 734.
[12] J. Schreuer, *IEEE T Ultrason. Ferr.* **2002**, *49*, 1474.
[13] E. Sun, S. Zhang, J. Luo, T. R. Shrout, W. Cao, *Appl. Phys. Lett.* **2010**, *97*, 032902.
[14] R. Zhang, B. Jiang, W. H. Jiang, W. Cao, *Mater. Lett.* **2003**, *57*, 1305.
[15] X. Liu, S. Zhang, J. Luo, T. R. Shrout, W. Cao, *Appl. Phys. Lett.* **2010**, *96*, 012907.
[16] C. He, W. Jing, F. Wang, K. Zhu, J. Qiu, *IEEE T Ultrason. Ferr.* **2011**, *58*, 1127.
[17] C. Chen, Y. Xiang, L. Tang, X. Li, L. Qin, W. Cao, *J. Mater. Sci.* **2020**, *55*, 12737.
[18] S. ANSI/IEEE, *IEEE standard on piezoelectricity*, IEEE, New York **1987**.
[19] A. W. Warner, M. Onoe, G. A. Coquin, *J Acoust. Soc. Am.* **1967**, *42*, 1223.
[20] B. A. Auld, *Acoustic Fields and Waves in Solids*, Krieger Publishing Company, Malabar, Florida **1990**.
[21] Y. Pang, Y. S. Wang, J. X. Liu, D. N. Fang, *Int. J. Eng. Sci.* **2008**, *46*, 1098.
[22] X. Yuan, Z. H. Zhu, *Acta. Mech.* **2012**, *223*, 2509.

